analytical chemistry

Article

pubs.acs.org/ac

Microsecond Protein Folding Events Revealed by Time-Resolved Fluorescence Resonance Energy Transfer in a Microfluidic Mixer

Liguo Jiang,[†] Yan Zeng,[‡] Qiqi Sun,[‡] Yueru Sun,[§] Zhihong Guo,[§] Jianan Y. Qu,*[,‡,▽] and Shuhuai Yao*[,⊥,▽]

[†]HKUST Jockey Club Institute for Advanced Study, [‡]Department of Electronic and Computer Engineering, [§]Department of Chemistry, [⊥]Department of Mechanical and Aerospace Engineering, and [▽]Division of Biomedical Engineering, Hong Kong University of Science and Technology, Hong Kong

Supporting Information

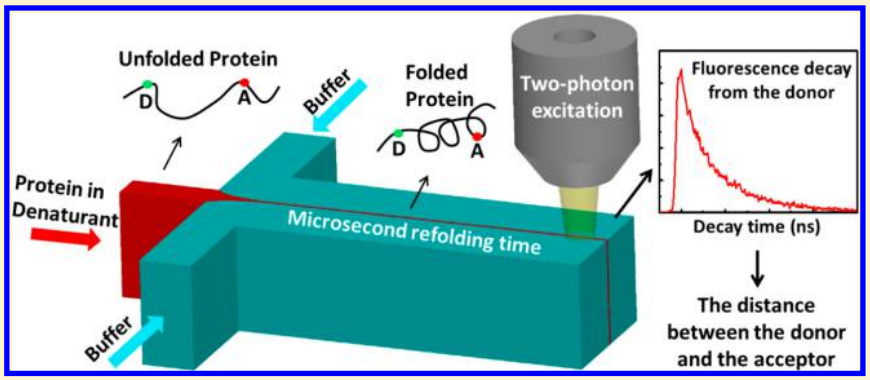

ABSTRACT: We demonstrate the combination of the time-resolved fluorescence resonance energy transfer (tr-FRET) measurement and the ultrarapid hydrodynamic focusing microfluidic mixer. The combined technique is capable of probing the intermolecular distance change with temporal resolution at microsecond level and structural resolution at Angstrom level, and the use of two-photon excitation enables a broader exploration of FRET with spectrum from near-ultraviolet to visible wavelength. As a proof of principle, we used the coupled microfluidic laminar flow and time-resolved two-photon excitation microscopy to investigate the early folding states of Cytochrome c (cyt c) by monitoring the distance between the tryptophan (Trp-59)-heme donor−acceptor (D−A) pair. The transformation of folding states of cyt c in the early 500 μs of refolding was revealed on the microsecond time scale. For the first time, we clearly resolved the early transient state of cyt c, which is populated within the dead time of the mixer (<10 μs) and has a characteristic Trp-59-heme distance of ∼31 Å. We believe this tool can find more applications in studying the early stages of biological processes with FRET as the probe.

Early folding pathways of proteins are, perhaps, the most important—yet poorly understood—events in the protein folding science. Within the first few milliseconds of the folding time domain, many proteins have already fulfilled their primary conformational changes. In the past few decades, progress in understanding of those early events has been largely promoted by the development of experimental tools to rapidly initiate the folding reactions, including temperature/pressure-jump,[1−4] photochemical triggers,[5,6] and rapid mixing methods.[7−12] Correspondingly, many physical probes have been used to monitor protein folding, including fluorescence,[4,9,10] absorption,[5] Förster resonance energy transfer (FRET),[13,14] small-angle X-ray scattering (SAXS),[3,15,16] circular dichroism (CD),[6,7,12] nuclear magnetic resonance (NMR),[17,18] time-resolved Fourier transform infrared (FT-IR) spectroscopy,[8] Raman spectroscopy,[19,20] etc. Appropriate combination of these detection techniques with rapid initiation methods often provides us valuable insight into protein folding with remarkable temporal and structural resolution.

The most extensively used method for initiating protein folding/unfolding is the rapid mixing, by which the solvent condition, such as denaturant concentration or pH, experiences a sudden jump. Stopped-flow mixing,[7] which relies on turbulence to achieve fast mixing, has been commonly used to study the protein folding kinetics. However, a burst phase phenomenon[21] is frequently observed in the stopped-flow measurement, because of the millisecond dead time of the device. Continuous-flow mixing reduces the dead time to 45 μs,[22] but a significant amount of sample consumption makes it less favorable. In contrast, ultrarapid microfluidic mixing, either by hydrodynamic flow focusing or by chaotic flow, greatly reduces the sample consumption to femtomole level and the mixing time to a few microseconds.[11,23−26] Nevertheless, many structural probes are difficult to be integrated with microfluidic mixing, because of the small amount of protein sample in the detection volume.[27−29]

Received: January 28, 2015
Accepted: May 4, 2015
Published: May 4, 2015

DOI: 10.1021/acs.analchem.5b00366
Anal. Chem. 2015, 87, 5589−5595

Recently, FRET measurement has attracted more and more attention in protein folding science,[13,30−32] because FRET provides direct information about the intermolecular distance of a protein. According to Förster,[33] the rate of the excitation energy transfer is proportional to the inverse sixth power of the distance between the donor and the acceptor, making the FRET measurement very sensitive to the protein structure at the angstrom (Å) level (∼10 Å to ∼100 Å).[34,35] Therefore, the FRET measurement has the promise to indicate protein structural change at Angstrom resolution. The steady-state FRET (ss-FRET), where fluorescence intensity is recorded for the change of the D−A distance, has been integrated with the hydrodynamic focusing microfluidic mixer for kinetic studies of Acyl−CoA binding protein (ACBP),[36] but the measured FRET efficiency only provides an average D−A distance along the protein folding pathway. While the FRET at single-molecule level is able to provide a more detailed structural distribution of the proteins,[14] it is hard to implement in ultrarapid mixing due to the extremely low signal provided by the protein molecule flowing through the detection spot at high speed. An alternative to the ss-FRET is the time-resolved FRET (tr-FRET) measurement,[37−39] by which the shape of the fluorescence decay curve is recorded. The tr-FRET provides more information than the ss-FRET because the decay curve is not only dependent on the average D−A distance but also on the D−A distance distribution and fluctuations.[40] It has been successfully demonstrated that coupling the tr-FRET measurement with the stopped-flow technique provided previously unachievable structural distribution features during the protein folding pathway.[41−44]

In this work, we coupled the tr-FRET measurement with hydrodynamic mixing to explore the early events in the horse Cytochrome c (cyt c) refolding.[45] We chose the Trp fluorescence for protein folding study because (i) most proteins contain intrinsically fluorescent Trp, or, even for proteins with no Trp residue or many Trp residues, they can be mutated by replacing a tyrosine residue with a Trp residue with little changes in overall stability and folding properties of the protein;[46] (ii) Trp fluorescence is very sensitive to its immediate environment, making it an ideal probe for monitoring the protein conformational changes;[47] (iii) besides the heme group, Trp can serve as a FRET donor for many other groups or residues, including the thionitrobenzoate,[44] tetracycline,[48] dansyl,[49] etc.; and (iv) Trp fluorescence in FRET shows predominantly a single exponential decay.[50−52] In our work, the Trp fluorescence decay curves were measured using a modified two-photon excited fluorescence (TPEF) and time-correlated single photon counting (TCSPC) system.[53] Normally, the Trp fluorescence must be excited by deep UV laser using single-photon excitation. Our two-photon excitation microscopy offers two distinct merits: First, using two-photon excitation of the Trp fluorescence allows the use of a visible wavelength laser, thus the device can be built in normal glass and silicon instead of fused silica, which substantially reduces the fabrication cost. Second, two-photon excitation can be a superior alternative to confocal microscopy. Two-photon excitation requires simultaneous absorption of two photons, which leads to fluorescence emission varying quadratically with the excitation intensity. In consequence, two-photon excitation is restricted to a tightly focused detection volume with a high degree of rejection of out-of-focus background fluorescence. The measured Trp fluorescence decays were analyzed using global fitting analysis[37,54] to obtain the D−A (Trp-59-heme) distance of subpopulated cyt c during refolding. The results show that, during the refolding pathway of cyt c within the first 500 μs time window, the transient state with a characteristic D−A distance of ∼31 Å and the folding intermediate state with a characteristic D−A distance of ∼22 Å are populated at ∼10 μs and ∼350 μs, respectively.

EXPERIMENTAL SECTION

Microfluidic Mixer. The mixer design was first described by Knight et al.,[11] optimized by Hertzog et al.,[23,24] and further improved by Yao et al.[25] The widths of nozzles at the center inlet channel, side inlet channels, and exit channel in our fabricated mixer are 2.2 ± 0.2 μm, 2.2 ± 0.2 μm, and 2.7 ± 0.2 μm, respectively. All microchannels of the mixer were etched 10.0 ± 0.4 μm in depth in a 525-μm-thick silicon wafer using deep reactive-ion etching (DRIE) (see Figure 1, inset), and liquid access holes were etched through the silicon wafers at the inlets and outlet using tetramethylammonium hydroxide (TMAH) etching with a 2500 Å thermal silicon oxide layer as a mask. The microchannels were sealed by anodic bonding with a 170-μm-thick Pyrex glass (SENSOR Prep Services, Inc.) and individual chips were diced using a wafer cutting machine. The flow rate of each channel was controlled by compressed air pressure above the liquid reservoir using LabVIEW (National Instruments) operated pressure transducers (Marsh Bellofram Type 2000, Newell, WV). In all experiments, the volumetric flow rates of sample and buffer were ∼2.8 μL/h and ∼280 μL/h, respectively. Such flow condition resulted in a maximum flow velocity of ∼1 m/s in the exit channel.

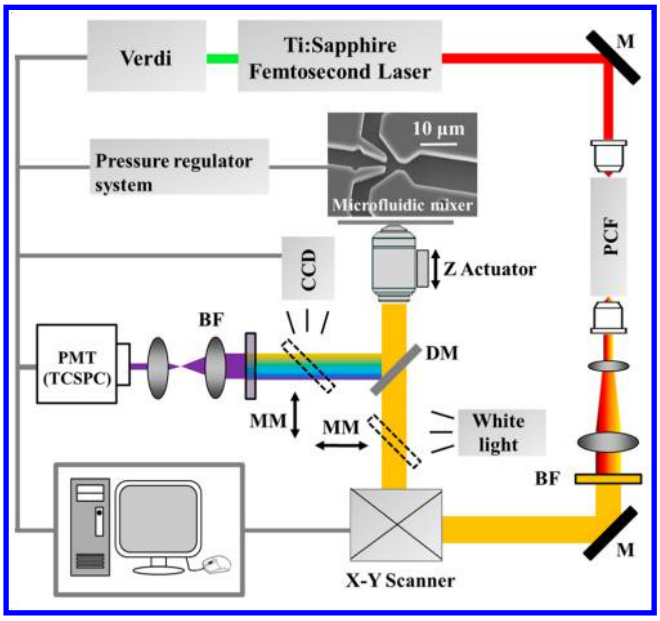

Figure 1. Schematic diagram of the time-resolved spectroscopic imaging system coupled with the microfluidic platform. Legend: PCF, photonic crystal fiber; M, mirror; DM, dichroic mirror; MM, movable mirror; BF, band-pass filter; and TCSPC, time-correlated single photon counting. The SEM image shows the fabricated hydrodynamic focusing mixer on a silicon substrate.

Optical System. The schematic diagram of the optical system is shown in Figure 1. To excite tryptophan fluorescence, the visible excitation source at 600 ± 20 nm was filtered out from the supercontinuum generated by a photonic crystal fiber (PCF) pumped by the femtosecond Ti:sapphire laser (Mira

DOI: 10.1021/acs.analchem.5b00366
Anal. Chem. 2015, 87, 5589−5595

900, coherent) operating at a repetition rate of 80 MHz (12.5 ns pulse separation). The fluctuation of supercontinuum spectrum was found to be within 1.5% and negligible. The collimated beam was then focused by a water immersion objective lens (UAPO40XW3/340, 1.15 NA, Olympus) of 250 μm working distance into the microchannel. The microscope imaging system produced lateral and axial resolutions of 0.5 and 1.5 μm, respectively. The backscattered signals were collected, filtered (FF01-357/44-25, Semrock) and directed to a telescope system, which guided the fluorescence signals to a single channel photomultiplier tube (PMT) equipped with a TCSPC module (PMC-100-4 and SPC-150, Becker & Hickl). To form a regular image at a certain depth, a pair of galvo mirrors was applied to create a rectangular sampling area. The imaging depth was determined by an actuator. The microfluidic mixer was mounted on a PC-controlled translation stage (V-102, Physik Instrument) with 0.1 μm positioning precision.

Materials. *N*-acetyltryptophan-amide (NATA) (A6501), horse heart Cytochrome c (C7752), and guanidine hydrochloride (GuHCl) (G3272) were purchased from Sigma–Aldrich and used without further modification. Apo-Cytochrome c (apo-cyt c) was prepared according to the method of Fisher et al.[55] In the characterization experiment, NATA was dissolved in 6 M GuHCl at 500 μM concentration and fed into the center channel. Potassium iodide (KI) was dissolved in phosphate-buffered saline (PBS, pH 7.4) at 100 mM concentration and fed into two side channels. In the equilibrium unfolding experiment, 500 μM concentration of cyt c and 50 μM concentration of apo-cyt c were dissolving in GuHCl of various concentrations, from 0 to 6 at 1 M interval. In the protein refolding experiment, 500 μM concentration of cyt c was unfolded by dissolving them in 6 M GuHCl. Folding was initiated by mixing them with 100 mM potassium phosphate buffer (PPB, pH 7.0) in the microfluidic mixer.

Data Analysis. The measured tr-FRET Trp fluorescence decay curves were first analyzed using single value decomposition (SVD).[56] The rank of the singular values determines the number of components that are required to compose those decay curves.[54,57] Global analysis[37,54] of fluorescence decay curves then was performed using the open source software Decayfit 1.4 (available at www.fluortools.com), in which the decay rate of each component is a fixed global parameter and the amplitude of each component is a varied local parameter. Those values are determined when the global chi-square (χ^2) goes minimum. The transformation to the D–A distance (r) then is readily accomplished by using the following equation:

$$k = k_0 + k_0\left(\frac{R_0}{r}\right)^6 \quad (1)$$

where k_0 is the donor fluorescence decay rate in the absence of acceptor and R_0 is the Förster distance between the donor and the acceptor, at which the energy transfer efficiency is 50%. In the study, the average Trp fluorescence decay rate k_0 of apo-cyt c[58] in water is $\sim 3 \times 10^8$ s^{-1} and the Förster distance R_0 is ~34 Å.[59] This Förster distance defines an r range of 10–51 Å ($0.3R_0 \leq r \leq 1.5R_0$) that can be probed. In this work, we used the global analysis to analyze the results, and all the obtained data were further analyzed using customer-built programs in MATLAB.

RESULTS AND DISCUSSION

System Characterization. The tr-FRET measurements were conducted in a laminar-flow mixer based on hydrodynamic focusing. The hydrodynamic focusing reduces the stream width to tens of nanometers for the molecules to diffuse and, consequently, lowers the mixing time to a few microseconds.[23−25] The stationary laminar flow offers an alternative means for examining the kinetics of a reaction, allowing the dynamic events in time history to be viewed at various points in the flow trajectory, enabling high temporal resolution in microscopy. We characterize the system using the diffusion-limited reaction of I ions quenching Trp fluorescence. Figure 2A shows the *N*-acetyltryptophan-amide (NATA) fluorescence

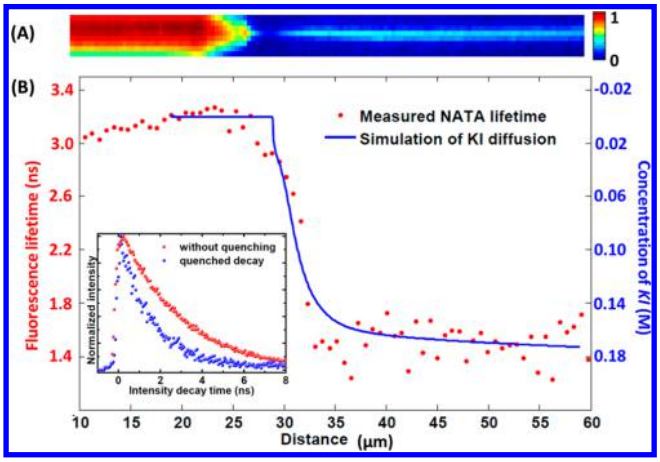

Figure 2. Characterization of the integrated system. (A) The jet showing the normalized fluorescence intensity of NATA in the microfluidic mixer. The captured image has an area of 90 μm × 6 μm. (B) Fluorescence lifetime change along the fluorescence jet. The fluorescence decay curves before and after NATA quenched by I ions (inset) show a fluorescence lifetime of 3.1 and 1.5 ns, respectively. The fluorescence lifetime is determined by minimizing the χ^2 value. The co-plotted blue line is the simulation of KI diffusion. Both results show a step change within ~10 μm, corresponding to a mixing time of ~6 ± 1 μs.

measured in the chip. At each pixel of the image, a fluorescence decay was collected as indicated in the inset. The change of NATA fluorescence lifetime along the jet (Figure 2B) is only caused by the quenching of Trp fluorescence, because of the rapid diffusion of I ions into the jet. The fluid flow and concentration fields in the mixer were simulated using Comsol Multiphysics 4.1 (Comsol, Inc.). The simulation result of the iodide ion diffusion into the focused jet (see Figure S1 in the Supporting Information) is indicated by the blue line. Both results show a step changing of the condition within ~10 μm, corresponding to ~6 ± 1 μs flow time or mixing time, estimated from the experiment and simulation.[25] Here, the mixing time is defined as the time when the concentration of KI in the simulation or the fluorescence lifetime of NATA in the experiment fulfills 90% change from the initial state to the final state.

Equilibrium Unfolding of Apo-cyt c and cyt c. We first tested the equilibrium unfolding of apo-cyt c in GuHCl of various concentrations. Almost identical Trp fluorescence decay curves of apo-cyt c (see Figure S2 in the Supporting Information) were observed, indicating that other than the Trp-59-heme D–A pair, the GuHCl concentration and the

DOI: 10.1021/acs.analchem.5b00366
Anal. Chem. 2015, 87, 5589−5595

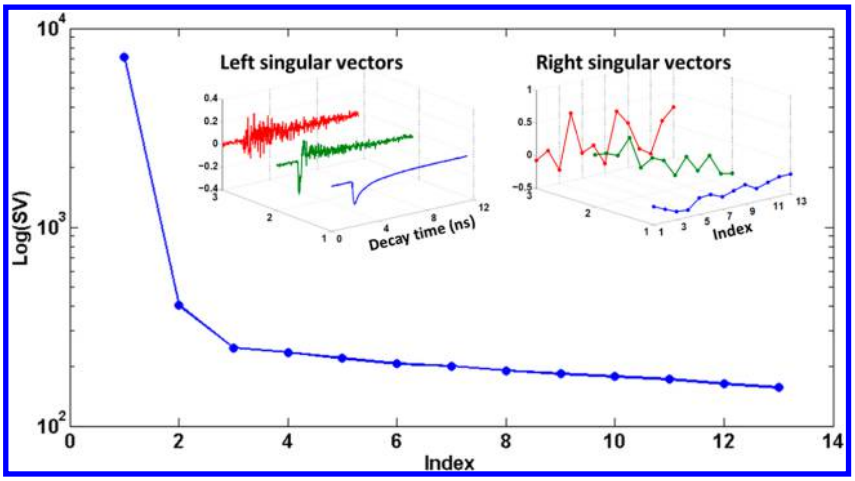

Figure 3. SVD analysis of measured Trp fluorescence decay curves. The singular values and associated left and right singular vectors (only three vectors are shown) roughly show no more than two independent components can be identified in the cyt c early refolding pathway. This result implies that a two-exponential decay model is suitable to capture the majority information on all Trp fluorescence decay curves. As the Trp fluorescence decay of cyt c shows predominantly a single exponential decay, this result also indicates that only two folding states of cyt c can be identified during the first 500 μs of the refolding time domain.

protein secondary structure, etc., do not contribute significantly to the Trp-59 fluorescence decay. Therefore, a constant k_0 in eq 1 can be employed to calculate the D−A distance during the cyt c unfolding and refolding at different concentrations of GuHCl and refolding times. We further examined the equilibrium unfolding of cyt c in GuHCl of various concentrations. The ensemble-averaged measurements of Trp fluorescence decay curves are shown in Figure S3 in the Supporting Information. SVD analysis of those decay curves indicates three significant components (Figure S4 in the Supporting Information). Co-plotted dashed black lines in Figure S3 in the Supporting Information are multiexponential fitting of the experimental data (convoluted with the instrument response function), and the fitting parameters are summarized in Table S1 in the Supporting Information. The results imply that a three-folding-state model is sufficient to describe the equilibrium unfolding of cyt c: the unfolded state with a decay rate of ~0.56 ns^{-1} (corresponding to a D−A distance of ~35 Å), the intermediate state with a decay rate of ~4.1 ns^{-1} (corresponding to a D−A distance of ~22 Å), and the native state with a decay rate of ~100 ns^{-1} (corresponding to a D−A distance of ~13 Å).

Kinetic Measurements of Cyt c Refolding. The cyt c refolding in the microfluidic mixer was initiated by rapid dilution of the denaturant (GuHCl) from the denatured condition at 6 M to the native condition at 0 M. During the refolding experiment, the Trp fluorescence decay along the jet was measured at different locations. Figure S5 in the Supporting Information shows the measured Trp fluorescence decays at various locations along the refolding trajectory. The changes of the Trp fluorescence decay rate along the cyt c refolding time course reveals the conformational transition of cyt c during its refolding pathway. SVD analysis of those decay curves after rapid mixing (Figure 3) shows that no more than two significant components can be identified in the early refolding pathway of cyt c. As the Trp fluorescence decay of cyt c shows predominantly a single exponential decay in the present of the heme group,[52] this SVD analysis results indicate two folding states of cyt c during its first 500 μs refolding time domain. Therefore, a two-exponential decay model was used in the global analysis:

$$I(t) = a_1 \exp(-k_1 t) + a_2 \exp(-k_2 t) \quad (2)$$

Here, a_1 and a_2 represent the fraction of the two states (the sum is unity); k_1 and k_2 represent the fluorescence decay rates of the two states. They were determined in the global analysis when the global χ^2 of the fitting reached the minimum. The results of the global analysis are shown in Figure 4 and

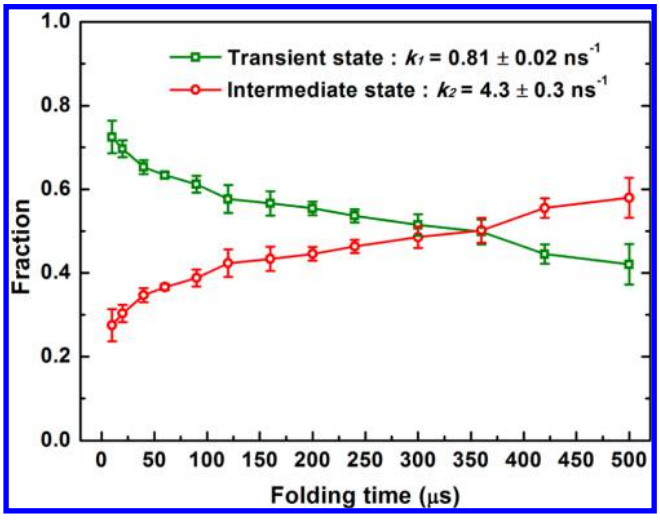

Figure 4. Global analysis of measured Trp fluorescence decay curves. Relative amplitudes of the two components vary during the cyt c refolding within 500 μs. Error bars (standard deviation) were calculated from three individual experiments.

summarized in Table S2 in the Supporting Information. The reconvolution of the fitting exponential decays with the instrument response function (IRF) was performed to ensure the accuracy of the global fitting (see Figure S5 in the Supporting Information). The first component (green line with square) has the shortest decay rate of 0.81 ± 0.02 ns^{-1}, corresponding to a D−A distance of ~31 Å (calculated from eq 1), which is significantly different from the unfolded state of cyt c with the D−A distance of ~35 Å[59] and the intermediate state of cyt c with the D−A distance of ~22 Å. Hence, we attribute this component to the transient state of cyt c. This transient

DOI: 10.1021/acs.analchem.5b00366
Anal. Chem. 2015, 87, 5589−5595

state is rapidly populated just after mixing in the cyt c refolding pathway, holding a fraction of ~0.7 of the total cyt c, and gradually decreases in the following time domain. The second component (red line with circle) has a decay rate of 4.3 ± 0.3 ns^{-1}, corresponding to a D−A distance of ~22 Å, which is comparable with the decay rate of 4.1 ns^{-1} for the intermediate state of cyt c. Hence, we attribute this component to the intermediate state of cyt c in its refolding pathway. The amplitude of the intermediate state gradually increases and becomes dominant after ~350 μs.

Based on the analysis, we schematically map the early refolding pathway of cyt c as shown in Figure 5. According to

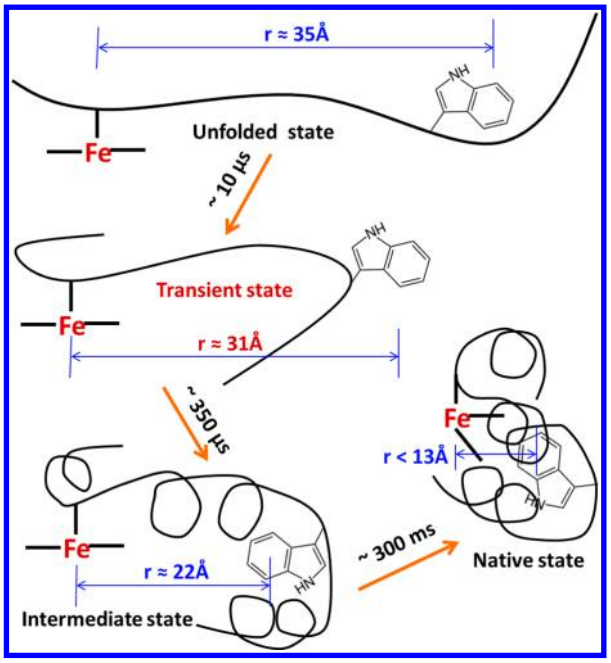

Figure 5. Schematic of the cyt c refolding deduced from our results and those of others.[10,16,27,60,61] Two transitional states (at ~10 μs and ~350 μs) were identified from our data. Highlighted in red is the early transient state of cyt c, populated within the dead time of the mixer (<10 μs) with a characteristic Trp-59-heme distance of ~31 Å, which was previously unresolved.

the previous study of the Trp fluorescence spectrum of cyt c in a microfluidic mixer,[27] the transient state resolved here is probably the hydrophobic collapsed state in the early refolding pathway. We depict the unfolded protein undergoing rapid transition within the first 10 μs refolding time domain. The resolved transient state of cyt c shows that the transition only shortens ~4 Å of the Trp-59-heme distance, from ~35 Å to ~31 Å. The change of the D−A distance results in the FRET efficiency shift from 0.46 to 0.64 (see the Supporting Information). The result also clearly indicates that a molten globule is generally populated in the 10−500 μs refolding time domain with a characteristic Trp-59-heme distance of ~22 Å. No native protein was found during this time domain, which implies that the populated molten globule is the on-pathway folding intermediate of cyt c and a significant energy barrier exists between the intermediate and native states.

The mapped cyt c early refolding pathway is in good agreement with previous studies. Shastry and Roder[10] measured the quenching of Trp fluorescence in cyt c using the continuous-flow mixing covering a time window from 45 μs to 900 μs, in which the observed kinetics exhibits two distinct exponential decays with time constants of 57 ± 5 μs and 430 ± 35 μs, respectively. It is interesting to note that the Trp fluorescence intensity decreased to ~65% of its original intensity in the unfolded state during the mixing dead time, which is very consistent with the intensity change calculated from our result (see the Supporting Information). Besides, Kathuria et al.[60] investigated the early refolding of cyt c in a continuous-flow mixer with mixing time of ~30 μs by measuring the Trp fluorescence lifetime. Although the fluorescence lifetime decay rates were quite different between their work and ours, because of the quenching of Trp fluorescence by imidazole[61] in their work, the number, transition time scale, and fraction of cyt c early folding states matched fairly well. However, the fluorescence lifetime decay that we resolved can provide correct conversion to the Trp59-heme distance to interpret the conformation change in cyt c refolding, because our measured Trp fluorescence was not interfered by the imidazole quenching. In addition, Lapidus et al.[27] observed the Trp-59 fluorescence spectral shift within the mixing time (~10 μs) and a spectral shift between ~100 μs in a microfluidic mixer. Other than the Trp fluorescence measurement, both the time-resolved CD measurement[62] and time-resolved SAXS measurement[16] of the cyt c refolding in continuous-flow mixers showed that the refolding of cyt c proceeded the sequential folding pathway with two monomeric intermediates with the folding rates of 12 500 s^{-1} from the unfolded state to intermediate I (corresponding to the transient state in our result), 2400 s^{-1} from the intermediate I to the intermediate II, and 68 s^{-1} from intermediate II to the native state. More recent fluorescence correlation spectroscopy (FCS) study[63] of the cyt c conformational fluctuations showed that the extend cyt c fluctuation into and out of the intermediate I occurred on a time scale of ~30 μs. The conformational transition time scale of our mapped cyt c early refolding pathway is fairly consistent with those results: ~10 μs for the transient state and ~350 μs for the folding intermediate state. The protein conformational change at ~10 μs is likely due to the nonspecific hydrophobic collapse, as supported by the CD measurement in which the α-helical contents of the intermediate I and the unfolded states are almost identical.[60] Furthermore, the absence of the native conformation during the intermediate state populated in our cyt c refolding map was verified by the hydrogen/deuterium (H/D) study.[16]

CONCLUSIONS

In conclusion, we visualize the Cytochrome c (cyt c) early refolding pathway from the time-resolved fluorescence resonance energy transfer (tr-FRET) of the Trp-59-heme pair by leveraging the advantages of microfluidic laminar flow mixing and scanning two-photon excitation microscopy. The developed technology allows us to map the early refolding pathway of cyt c with microsecond temporal resolution and Angstrom level structural change. For the first time, we directly probed the transient state of cyt c, which is only a slight decrease of the Trp-59-heme distance while increasing the FRET efficiency from ~0.46 to ~0.64. When unfolded cyt c is rapidly triggered to refold, the extend conformation experiences a fast transition within 10 μs to a transient state with a characteristic Trp-59-heme distance of ~31 Å. Later, the protein chain further compacts and a folding intermediate with a characteristic Trp-59-heme distance of ~22 Å is generally populated and becomes dominant after ~350 μs. In principle, this combined tool can also be used to investigate any

DOI: 10.1021/acs.analchem.5b00366
Anal. Chem. 2015, 87, 5589−5595

macromolecule conformational changes such as RNA folding, molecular interactions in enzyme catalysis, and protein−protein interactions on the microsecond time scale, as long as those biological systems possess FRET probes.

■ ASSOCIATED CONTENT

Supporting Information

Additional information as noted in text. The Supporting Information is available free of charge on the ACS Publications website at DOI: 10.1021/acs.analchem.5b00366.

■ AUTHOR INFORMATION

Corresponding Authors

*E-mail: eequ@ust.hk (J. Y. Qu).
*E-mail: meshyao@ust.hk (S. Yao).

Notes

The authors declare no competing financial interest.

■ ACKNOWLEDGMENTS

The authors thank the Nanoelectronics Fabrication Facility at HKUST for their technical support. This work was supported by RGC General Research Fund (No. 621113).

■ REFERENCES

(1) Sabelko, J.; Ervin, J.; Gruebele, M. *Proc. Natl. Acad. Sci. U.S.A.* **1999**, *96*, 6031−6036.
(2) Thompson, P. A.; Eaton, W. A.; Hofrichter, J. *Biochemistry* **1997**, *36*, 9200−9210.
(3) Woenckhaus, J.; Kohling, R.; Thiyagarajan, P.; Littrell, K. C.; Seifert, S.; Royer, C. A.; Winter, R. *Biophys. J.* **2001**, *80*, 1518−1523.
(4) Jacob, M.; Holtermann, G.; Perl, D.; Reinstein, J.; Schindler, T.; Geeves, M. A.; Schmid, F. X. *Biochemistry* **1999**, *38*, 2882−2891.
(5) Jones, C. M.; Henry, E. R.; Hu, Y.; Chan, C. K.; Luck, S. D.; Bhuyan, A.; Roder, H.; Hofrichter, J.; Eaton, W. A. *Proc. Natl. Acad. Sci. U.S.A.* **1993**, *90*, 11860−11864.
(6) Chen, E.; Wood, M. J.; Fink, A. L.; Kliger, D. S. *Biochemistry* **1998**, *37*, 5589−5598.
(7) Kuwajima, K.; Yamaya, H.; Miwa, S.; Sugai, S.; Nagamura, T. *FEBS Lett.* **1987**, *221*, 115−118.
(8) Fabian, H.; Naumann, D. *Methods* **2004**, *34*, 28−40.
(9) Chan, C. K.; Hu, Y.; Takahashi, S.; Rousseau, D. L.; Eaton, W. A.; Hofrichter, J. *Proc. Natl. Acad. Sci. U.S.A.* **1997**, *94*, 1779−1784.
(10) Shastry, M. R.; Roder, H. *Nat. Struct. Biol.* **1998**, *5*, 385−392.
(11) Knight, J. B.; Vishwanath, A.; Brody, J. P.; Austin, R. H. *Phys. Rev. Lett.* **1998**, *80*, 3863−3866.
(12) Kane, A. S.; Hoffmann, A.; Baumgartel, P.; Seckler, R.; Reichardt, G.; Horsley, D. A.; Schuler, B.; Bakajin, O. *Anal. Chem.* **2008**, *80*, 9534−9541.
(13) Lipman, E. A.; Schuler, B.; Bakajin, O.; Eaton, W. A. *Science* **2003**, *301*, 1233−1235.
(14) Gambin, Y.; VanDelinder, V.; Ferreon, A. C. M.; Lemke, E. A.; Groisman, A.; Deniz, A. A. *Nat. Methods* **2011**, *8*, 239−241.
(15) Pollack, L.; Tate, M. W.; Darnton, N. C.; Knight, J. B.; Gruner, S. M.; Eaton, W. A.; Austin, R. H. *Proc. Natl. Acad. Sci. U.S.A.* **1999**, *96*, 10115−10117.
(16) Akiyama, S.; Takahashi, S.; Kimura, T.; Ishimori, K.; Morishima, I.; Nishikawa, Y.; Fujisawa, T. *Proc. Natl. Acad. Sci. U.S.A.* **2002**, *99*, 1329−1334.
(17) Dyson, H. J.; Wright, P. E. *Chem. Rev.* **2004**, *104*, 3607−3622.
(18) Balbach, J.; Forge, V.; Nuland, N. A. J.; Winder, S. L.; Hore, P. J.; Dobaon, C. M. *Nat. Struct. Biol.* **1995**, *2*, 865−870.
(19) Lednev, I. K.; Karnoup, A. S.; Sparrow, M. C.; Asher, S. A. *J. Am. Chem. Soc.* **1999**, *121*, 8074−8086.
(20) Takahashi, S.; Yeh, S. R.; Das, T. K.; Chan, C. K.; Gottfried, D. S.; Rousseau, D. L. *Nat. Struct. Biol.* **1997**, *4*, 44−50.
(21) Qi, P. X.; Sosnick, T. R.; Englander, S. W. *Nat. Struct. Biol.* **1998**, *5*, 882−884.
(22) Shastry, M.; Luck, S. D.; Roder, H. *Biophys. J.* **1998**, *74*, 2714−2721.
(23) Hertzog, D. E.; Michalet, X.; Jager, M.; Kong, X.; Santiago, J. G.; Weiss, S.; Bakajin, O. *Anal. Chem.* **2004**, *76*, 7169−7178.
(24) Hertzog, D. E.; Ivorra, B.; Mohammadi, B.; Bakajin, O.; Santiago, J. G. *Anal. Chem.* **2006**, *78*, 4299−4306.
(25) Yao, S.; Bakajin, O. *Anal. Chem.* **2007**, *79*, 5753−5759.
(26) Waldauer, S. A.; Bakajin, O.; Lapidus, L. J. *Proc. Natl. Acad. Sci. U.S.A.* **2010**, *107*, 13713−13717.
(27) Lapidus, L. J.; Yao, S.; McGarrity, K. S.; Hertzog, D. E.; Tubam, E.; Bakajin, O. *Biophys. J.* **2007**, *93*, 218−224.
(28) DeCamp, S. J.; Naganathan, A. N.; Waldauer, S. A.; Bakajin, O.; Lapidus, L. J. *Biophys. J.* **2009**, *97*, 1772−1777.
(29) Wu, L.; Lapidus, L. J. *Anal. Chem.* **2013**, *85*, 4920−4924.
(30) Schuler, B.; Eaton, W. A. *Curr. Opin. Struc. Biol.* **2008**, *18*, 16−26.
(31) Deniz, A. A.; Laurence, T. A.; Beligere, G. S.; Dahan, M.; Martin, A. B.; Chemia, D. S.; Dawson, P. E.; Schultz, P. G.; Weiss, S. *Proc. Natl. Acad. Sci. U.S.A.* **2009**, *97*, 5179−5184.
(32) Schuler, B.; Lipman, E. A.; Eaton, W. A. *Nature* **2002**, *419*, 743−747.
(33) Főrster, T. *Discuss. Faraday Soc.* **1959**, *27*, 7−17.
(34) Selvin, P. R. *Nat. Struct. Biol.* **2000**, *7*, 730−734.
(35) Clegg, R. M. *Curr. Opin. Biotechnol.* **1995**, *6*, 103−110.
(36) Voelz, V. A.; Jager, M.; Yao, S.; Chen, Y.; Zhu, L.; Waldauer, S. A.; Bowman, G. R.; Friedrichs, M.; Bakajin, O.; Lapidus, L.; Weiss, S.; Pande, V. S. *J. Am. Chem. Soc.* **2012**, *134*, 12565−12577.
(37) Huang, F.; Lerner, E.; Sato, S.; Amir, D.; Haas, E.; Fersht, A. R. *Biochemistry* **2009**, *48*, 3468−3476.
(38) Gopich, I. V.; Szabo, A. *Proc. Natl. Acad. Sci. U.S.A.* **2012**, *109*, 7747−7752.
(39) Klostermeier, D.; Millar, D. P. *Biopolymers* **2002**, *61*, 159−179.
(40) Haas, E.; Katchalski-Katzir, E.; Steinberg, I. Z. *Biochemistry* **1978**, *17*, 5064−5070.
(41) Lyubovitsky, J. G.; Gray, H. B.; Winkler, J. R. *J. Am. Chem. Soc.* **2002**, *124*, 5481−5485.
(42) Lee, J. C.; Engman, K. C.; Tezcan, F. A.; Gray, H. B.; Winkler, J. R. *Proc. Natl. Acad. Sci. U.S.A.* **2002**, *99*, 14778−14782.
(43) Pletneva, E. V.; Gray, H. B.; Winkler, J. R. *Proc. Natl. Acad. Sci. U.S.A.* **2005**, *102*, 18397−18402.
(44) Jha, S. K.; Dhar, D.; Krishnamoorthy, G.; Udgaonkar, J. B. *Proc. Natl. Acad. Sci. U.S.A.* **2009**, *106*, 11113−11118.
(45) Goldbeck, R. A.; Chen, E.; Kliger, D. S. *Int. J. Mol. Sci.* **2009**, *10*, 1476−1499.
(46) Vallée-Bélisle, A.; Michnick, S. W. *Nat. Struct. Biol.* **2012**, *19*, 731−736.
(47) Chen, Y.; Barkley, M. D. *Biochemistry* **1998**, *37*, 9976−9982.
(48) Beierlein, F. R.; Othersen, O. G.; Lanig, H.; Schneider, S.; Clark, T. *J. Am. Chem. Soc.* **2006**, *128*, 5142−5152.
(49) Deng, W.; Cao, A.; Lai, L. *Protein Sci.* **2008**, *17*, 1102−1105.
(50) Hochstrasser, R. M.; Negus, D. K. *Proc. Natl. Acad. Sci.* **1984**, *81*, 4399−4403.
(51) Das, T. K.; Mazumdar, S. *Eur. J. Biochem.* **1995**, *227*, 823−828.
(52) Das, T. K.; Mazumdar, S.; Mitra, S. *Eur. J. Biochem.* **1998**, *254*, 662−670.
(53) Li, D.; Zheng, W.; Qu, J. Y. *Opt. Lett.* **2009**, *34*, 202−204.
(54) Laptenok, S. P.; Visser, N. V.; Engel, R.; Westphal, A. H.; Van Hoek, A.; Van Mierlo, C. P. M.; Van Stokkum, I. H. M.; Van Amerongen, H.; Visser, A. J. W. G. *Biochemistry* **2011**, *50*, 3441−3450.
(55) Fisher, W. R.; Taniuchi, H.; Anfinsen, C. B. *J. Biol. Chem.* **1973**, *248*, 3188−3195.
(56) Henry, E. R.; Hofrichter, J. *Methods Enzymol.* **1992**, *210*, 129−192.
(57) Van Stokkum, I. H. M.; Larsen, D. S.; van Grondelle, R. *Biochim. Biophys. Acta, Bioenerg.* **2004**, *1657*, 82−104.
(58) Vincent, M.; Brochon, J. C.; Merola, F.; Jordi, W.; Gallay, J. *Biochemistry* **1998**, *27*, 8752−8761.

DOI: 10.1021/acs.analchem.5b00366
Anal. Chem. 2015, 87, 5589−5595

(59) Sanchez, K. M.; Schlamadinger, D. E.; Gable, J. E.; Kim, J. E. *J. Chem. Educ.* **2008**, *85*, 1253−1256.
(60) Kathuria, S. V.; Kayatekin, C.; Barrea, R.; Kondrashkina, E.; Graceffa, R.; Guo, L.; Nobrega, R. P.; Chakravarthy, S.; Matthews, C. R.; Irving, T. C.; Bilsel, O. *J. Mol. Biol.* **2014**, *426*, 1980−1994.
(61) Willaert, K.; Engelborghs, Y. *Eur. Biophys. J.* **1991**, *20*, 177−182.
(62) Akiyama, S.; Takahashi, S.; Ishimori, K.; Morishima, I. *Nat. Struct. Biol.* **2000**, *7*, 514−520.
(63) Werner, J. H.; Joggerst, R.; Dyer, R. B.; Goodwin, P. M. *Proc. Natl. Acad. Sci. U.S.A.* **2006**, *103*, 11130−11135.

DOI: 10.1021/acs.analchem.5b00366
Anal. Chem. 2015, 87, 5589−5595